Int. J. Heat Mass Transfer. Vol. 34, No. 2, pp. 377–388, 1991
Printed in Great Britain

0017-9310/91 $3.00+0.00

Natural-convection flow in a square cavity calculated with low-Reynolds-number turbulence models

R. A. W. M. HENKES, F. F. VAN DER VLUGT and C. J. HOOGENDOORN
Department of Applied Physics, Delft University of Technology,
P.O. Box 5046, 2600 GA Delft, The Netherlands

(*Received* 4 *September* 1989)

Abstract—The laminar and turbulent natural-convection flow in a two-dimensional square cavity heated from the vertical side is numerically calculated up to a Rayleigh number of 10^{14} for air and up to 10^{15} for water. Three different turbulence models are compared: the standard k–ε model with logarithmic wall functions and the low-Reynolds-number models of Chien, and Jones and Launder. The position of the laminar–turbulent transition in the vertical boundary layer strongly depends on the turbulence model used. Moreover, multiple solutions for the transition position can occur for a fixed Rayleigh number at the same numerical grid. The thermal stratification in the core of the cavity breaks up when the flow becomes turbulent. Comparison of the averaged wall-heat transfer with experiments for the hot vertical plate and for tall vertical cavities shows that the standard k–ε model gives a too high prediction, whereas the low-Reynolds-number models are reasonably close to the experiment.

1. INTRODUCTION

A TEMPERATURE difference over the vertical sides of a cavity gives rise to the natural-convection flow of the fluid inside. If the Rayleigh number, which is a characteristic number of the problem, exceeds a critical value the laminar flow can become turbulent. Because the direct numerical simulation of the turbulent flow by solving the full unsteady, three-dimensional Navier–Stokes equations is beyond the possibilities of present-day computers, the turbulence has to be modelled. A well-known turbulence model is the k–ε model.

When the flow is turbulent the Rayleigh number is large ($> 10^9$ for air). For these large Rayleigh numbers the flow has thin boundary layers along the vertical sides of the cavity. The core of the cavity is thermally stratified. In the part of the vertical boundary layer closest to the wall, gradients in the flow are very large and require the use of many computational grid points. In most turbulence calculations the solution in this part of the boundary layer is approximated by 'universal profiles': the logarithmic wall functions. These logarithmic wall functions were originally derived, and experimentally verified, for forced-convection flows (for example the boundary-layer flow along a plate in an oncoming velocity field). The logarithmic wall functions do not hold for natural-convection boundary layers. However, because of lack of better wall functions, they still are often used in natural-convection problems. The search for the right wall functions for natural-convection boundary layers is going on [1–3].

Instead of using wall functions, it is also possible to solve the flow equations up to the wall. The large damping of the turbulence in the wall region requires a modification of the standard k–ε model. A lot of such modified models, the so-called low-Reynolds-number k–ε models, have been proposed in the literature. In ref. [4] all these models have been compared for the flow of air along an elemental natural-convection configuration, namely the hot vertical plate in an isothermal environment. The low-Reynolds-number models of Lam and Bremhorst, Chien, and Jones and Launder turned out to predict the wall-heat transfer closest to the experimental value. The use of the standard k–ε model with logarithmic wall functions for k and ε gives a 30% too high prediction.

Another elemental natural-convection configuration is the square cavity heated from the vertical side. The boundary layer along the hot vertical side of the cavity shows a close resemblance with the boundary layer along a hot vertical plate in a stratified environment. In the present study we have calculated the flow of air and water in the two-dimensional, square cavity for a Rayleigh number up to 10^{15}. The performance of the standard k–ε model with (logarithmic) wall functions, the low-Reynolds-number k–ε model of Chien [5] and the low-Reynolds-number k–ε model of Jones and Launder [6] are compared. Calculations in the square cavity with the standard k–ε model with wall functions have also been made for air by Markatos and Pericleous [7] and for water by Ozoe *et al.* [8]. Ince and Launder [9] have recently used the Jones and Launder model to calculate the turbulent flow of air in tall vertical cavities.

A difficulty is that accurate experiments for the turbulent flow in the square cavity do not exist. We have used the experimental wall-heat transfer for very tall cavities and for the hot vertical plate in an isothermal environment to make a guess of the exper-

NOMENCLATURE

A	aspect ratio, height/width
c_f	dimensionless wall-shear stress, $2\nu(\partial v/\partial x)_w/g\beta\Delta TH$
$c_{1\varepsilon}$, $c_{2\varepsilon}$, $c_{3\varepsilon}$	coefficients in ε-equation
c_μ	coefficient in ν_t-equation
D	low-Reynolds-number source term in k-equation
E	low-Reynolds-number source term in ε-equation
f	frequency
f_1	low-Reynolds-number correction for $c_{1\varepsilon}$
f_2	low-Reynolds-number correction for $c_{2\varepsilon}$
f_μ	low-Reynolds-number correction for c_μ
g	gravitational acceleration
G_k	buoyancy production of turbulent kinetic energy
H	height of the cavity
k	turbulent kinetic energy
Nu	Nusselt number at hot wall, $-H/\Delta T[\partial T/\partial x]_w$
$\overline{Nu}$	averaged Nusselt number at hot wall, $\int_0^1 Nu\, d(y/H)$
p	pressure
p'	pressure correction in numerical iteration
P_k	shear production of turbulent kinetic energy
Pr	Prandtl number
Ra	Rayleigh number, $g\beta\Delta TH^3\, Pr/\nu^2$
Re_t	turbulent Reynolds number, $k^2/\nu\varepsilon$
S	gradient of thermal stratification in cavity centre, $H/\Delta T[\partial T/\partial y]$
t	time
Δt	numerical time step
T	temperature
ΔT	characteristic temperature difference, $T_h - T_c$
T_h	temperature of hot wall
T_c	temperature of cold wall
u	horizontal velocity component
u_t	velocity component tangential to closest fixed wall
u_τ	characteristic shear-stress velocity, $\sqrt{(\nu(\partial u_t/\partial y_n)_w)}$
v	vertical velocity component
x	horizontal coordinate
y	vertical coordinate
y_n	distance to closest fixed wall
y_{tr}	position of transition for hot vertical boundary layer
y^+	dimensionless coordinate, $y_n u_\tau/\nu$.

Greek symbols

α_1, α_2	coefficients in function for grid-point distribution
β	coefficient of thermal expansion
ε	rate of dissipation of turbulent kinetic energy
ν	molecular kinematic viscosity
ν_t	turbulent kinematic viscosity
ρ	density
σ_k	turbulent Prandtl number for k
σ_T	turbulent Prandtl number for T
σ_ε	turbulent Prandtl number for ε.

Superscript

n	time level.

Subscripts

i	grid point in the x-direction
j	grid point in the y-direction
max	maximum of a quantity
w	wall condition.

imental averaged wall-heat transfer through the vertical side of the square cavity. The prediction of the different models is compared with this experimental value.

We will also discuss that the solution for the low-Reynolds-number k–ε models can be nonunique. For a fixed Rayleigh number, both converged solutions with an early and a late transition from the laminar to the turbulent state in the boundary layer have been calculated. Besides the averaged wall-heat transfer as a function of the Rayleigh number, we also present the following quantities as a function of height: wall-heat transfer, wall-shear stress, maximum of the vertical velocity, maximum of the turbulent viscosity, horizontal velocity at half the cavity width and the thermal stratification at half the cavity width.

2. MATHEMATICAL FORMULATION

We consider a square cavity, with fixed walls, that is differentially heated over the vertical sides. The left hot wall has a temperature T_h and the right cold wall has a temperature T_c. The horizontal floor and ceiling are both adiabatic. The height of the cavity is H. The x and y coordinates are chosen in the horizontal and vertical direction, respectively.

The two-dimensional laminar and turbulent flow in this square cavity is described by the Reynolds equations. It is assumed that the fluid is incompressible and satisfies the Boussinesq approximation

$$\frac{\partial u}{\partial x} + \frac{\partial v}{\partial y} = 0$$

$$\frac{\partial u}{\partial t}+u\frac{\partial u}{\partial x}+v\frac{\partial u}{\partial y}=-\frac{1}{\rho}\frac{\partial p}{\partial x}+\frac{\partial}{\partial x}(\nu+\nu_t)\left(2\frac{\partial u}{\partial x}\right)+\frac{\partial}{\partial y}(\nu+\nu_t)\left(\frac{\partial u}{\partial y}+\frac{\partial v}{\partial x}\right)$$

$$\frac{\partial v}{\partial t}+u\frac{\partial v}{\partial x}+v\frac{\partial v}{\partial y}=-\frac{1}{\rho}\frac{\partial p}{\partial y}+g\beta(T-T_c)+\frac{\partial}{\partial x}(\nu+\nu_t)\left(\frac{\partial v}{\partial x}+\frac{\partial u}{\partial y}\right)+\frac{\partial}{\partial y}(\nu+\nu_t)\left(2\frac{\partial v}{\partial y}\right)$$

$$\frac{\partial T}{\partial t}+u\frac{\partial T}{\partial x}+v\frac{\partial T}{\partial y}=\frac{\partial}{\partial x}\left(\frac{\nu}{Pr}+\frac{\nu_t}{\sigma_T}\right)\frac{\partial T}{\partial x}+\frac{\partial}{\partial y}\left(\frac{\nu}{Pr}+\frac{\nu_t}{\sigma_T}\right)\frac{\partial T}{\partial y}$$

$$\frac{\partial k}{\partial t}+u\frac{\partial k}{\partial x}+v\frac{\partial k}{\partial y}=\frac{\partial}{\partial x}\left(\nu+\frac{\nu_t}{\sigma_k}\right)\frac{\partial k}{\partial x}+\frac{\partial}{\partial y}\left(\nu+\frac{\nu_t}{\sigma_k}\right)\frac{\partial k}{\partial y}+P_k+G_k-\varepsilon+D$$

$$\frac{\partial \varepsilon}{\partial t}+u\frac{\partial \varepsilon}{\partial x}+v\frac{\partial \varepsilon}{\partial y}=\frac{\partial}{\partial x}\left(\nu+\frac{\nu_t}{\sigma_\varepsilon}\right)\frac{\partial \varepsilon}{\partial x}+\frac{\partial}{\partial y}\left(\nu+\frac{\nu_t}{\sigma_\varepsilon}\right)\frac{\partial \varepsilon}{\partial y}+(c_{1\varepsilon}f_1(P_k+c_{3\varepsilon}G_k)-c_{2\varepsilon}f_2\varepsilon)\frac{\varepsilon}{k}+E \quad (1)$$

with

$$P_k=\nu_t\left(2\left(\frac{\partial u}{\partial x}\right)^2+2\left(\frac{\partial v}{\partial y}\right)^2+\left(\frac{\partial u}{\partial y}+\frac{\partial v}{\partial x}\right)^2\right),$$

$$G_k=-\frac{\nu_t}{\sigma_T}g\beta\frac{\partial T}{\partial y},\quad \nu_t=c_\mu f_\mu\frac{k^2}{\varepsilon}.$$

These Reynolds equations are obtained by time-averaging the high-frequency turbulent fluctuations from the Navier–Stokes equations. It seems a bit strange that, despite the time-averaging, the unsteady terms remain in the formulation. However, the time-averaging is restricted to the broad-band spectrum of turbulence, whereas the remaining unsteady terms account for all weak unsteadiness that does not belong to the turbulence. We can also define that the unsteady terms represent all unsteadiness that is not modelled by the turbulence model. In this study we are interested in the large-time behaviour of the flow; we check whether all unsteadiness dies out and a steady final solution is reached. The Reynolds stresses appearing in the Reynolds equations have been modelled with the k–ε model. Three versions of the k–ε model are compared:

(i) Standard k–ε model with wall functions

$c_\mu=0.09$, $c_{1\varepsilon}=1.44$, $c_{2\varepsilon}=1.92$, $\sigma_T=1.0$, $\sigma_k=1.0$, $\sigma_\varepsilon=1.3$, $f_\mu=f_1=f_2=1.0$, $D=E=0$

wall functions at the first inner grid point: $k=u_\tau^2/\sqrt{(c_\mu)}$, $\varepsilon=u_\tau^4/0.41\nu y^+$.

(ii) Low-Reynolds-number k–ε model of Chien [5]

$c_\mu=0.09$, $c_{1\varepsilon}=1.35$, $c_{2\varepsilon}=1.8$, $\sigma_T=1.0$, $\sigma_k=1.0$, $\sigma_\varepsilon=1.3$, $f_\mu=1-\exp(-0.0115y^+)$,

$f_1=1.0$, $f_2=1-\frac{2}{9}\exp(-(Re_t/6)^2)$,

$D=-2\nu\frac{k}{y_n^2}$, $E=-\frac{2\nu\varepsilon}{y_n^2}\exp(-0.5y^+)$

at the wall: $k=\varepsilon=0$.

(iii) Low-Reynolds-number k–ε model of Jones and Launder [6]

$c_\mu=0.09$, $c_{1\varepsilon}=1.44$, $c_{2\varepsilon}=1.92$, $\sigma_T=0.9$, $\sigma_k=1.0$, $\sigma_\varepsilon=1.3$, $f_\mu=\exp\left(\frac{-2.5}{1+Re_t/50}\right)$,

$f_1=1.0$, $f_2=1-0.3\exp(-Re_t^2)$,

$$D=-2\nu\left[\left(\frac{\partial\sqrt{k}}{\partial x}\right)^2+\left(\frac{\partial\sqrt{k}}{\partial y}\right)^2\right],$$

$$E=2\nu\nu_t\left[\left(\frac{\partial^2 u}{\partial y^2}\right)^2+\left(\frac{\partial^2 v}{\partial x^2}\right)^2\right]$$

at the wall: $k=\varepsilon=0$.

In these relations the following dimensionless variables appear: $u_\tau=\sqrt{(\nu(\partial u_t/\partial y_n)_w)}$, $y^+=y_n u_\tau/\nu$ and $Re_t=k^2/\nu\varepsilon$ (y_n is the distance to the closest fixed wall and u_t the velocity component tangential to that wall). In model (i) the wall functions are only used to obtain boundary conditions for the k and ε equations. These expressions are based on the logarithmic wall functions as originally derived for forced-convection boundary layers. No wall functions are applied to the velocity and temperature profiles.

Rodi [10] has suggested that the coefficient $c_{3\varepsilon}$ is close to 1 in vertical boundary layers and close to 0 in horizontal boundary layers. An approximation that satisfies both limits is used in the present formulation

$$c_{3\varepsilon}=\tanh|v/u|. \quad (2)$$

In the literature there is still no consensus on the right formulation of $c_{3\varepsilon}$ and G_k. For example, Fraikin *et al.* [11] took $c_{3\varepsilon}=0.7/c_{1\varepsilon}$ and Ince and Launder [9] took $c_{3\varepsilon}=1$ in their turbulent cavity calculations. If the Rayleigh number is increased to infinity, the turbulent solution in the cavity consists of natural-convection boundary layers along the vertical walls and an almost stagnant, stably stratified core region (see Fig. 1). The streamlines in the core are practically horizontal. Turbulence is concentrated in the boundary layer and is almost absent in the core. The stability analysis (see, e.g. Nachtsheim [12]) for the laminar natural-convection boundary layer along a heated vertical plate in an isothermal environment shows that the critical gradients in both the velocity profile and the temperature profile can initiate an instability and the transition to turbulence (giving a hydrodynamic and thermal instability, respectively). The hydrodynamic instability mechanism is represented by the P_k-term in the k-equation, whereas the thermal instability mechanism is represented by the G_k-term. The stability analysis for the core (approximated as an inviscid,

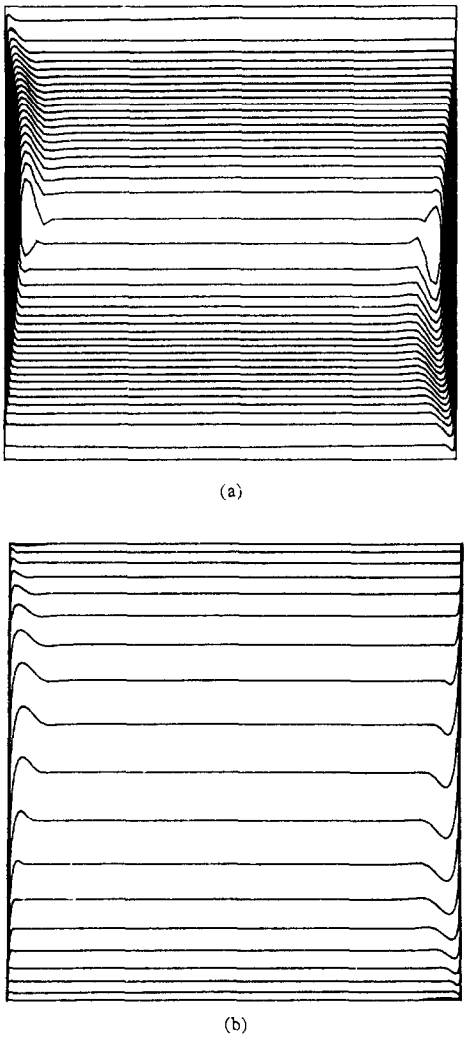

FIG. 1. Turbulent flow of air at $Ra = 10^{12}$ (Chien model): (a) streamlines; (b) isotherms.

stagnant, thermally stratified environment; see, e.g. Drazin and Reid [13]) shows that the thermal instability is only damped if the stratification is stable, i.e if the density decreases with height, or (provided $\beta > 0$) if the temperature increases with height. The present formulation for the thermal source G_k in the k-equation does not seem to be in line with these stability analyses. The source $c_{1\varepsilon}c_{3\varepsilon}G_k$ has the right sign in the stably stratified core, namely less than or equal to 0, but its value is everywhere close to zero. This is a consequence of the almost horizontal streamlines in the core, giving $c_{3\varepsilon} \sim 0$ according to equation (2). Therefore, it might be better to use $c_{3\varepsilon} = 1$ in the core. Because the y-derivatives in the vertical boundary layers are small compared to the x-derivatives, the present formulation gives $|G_k| \ll |P_k|$. This implies that the thermal instability mechanism is not accounted for very realistically in the vertical boundary layer. Ince and Launder [9] have proposed the inclusion of a $\partial T/\partial x$ contribution in the G_k-term. Actually the use of a Reynolds-stress model, instead of the k–ε model, automatically leads to such a contribution. Peeters and Henkes [14] have used the Reynolds-stress model for the turbulent natural-convection boundary layer along a heated vertical plate in an isothermal environment. In the inner layer (i.e. from the wall up to the velocity maximum) G_k is close to zero, but in the outer layer (i.e. beyond the velocity maximum) it is roughly 30% of the total production of turbulent kinetic energy. Because the corrected G_k-term gives rise to both an increase of k and ε, the overall influence on ν_t turns out to be small. Therefore, the use of the old formulation for G_k, as we still do in the present study, will not lead to large differences in quantities like the wall-heat transfer, the velocity maximum, the stratification, etc.

After nondimensionalization of the dependent and independent variables (with the help of H, $\Delta T = T_h - T_c$, $g\beta$ and ν), the solution in the square cavity depends only on two characteristic numbers: the Prandtl number (Pr) and the Rayleigh number ($Ra = g\beta\Delta T H^3 Pr/\nu^2$). The solution is centro-symmetric with respect to the centre of the cavity.

3. NUMERICAL PROCEDURE

The spatial derivatives in the equations are discretized with the finite-volume method on a staggered grid. The solution domain is covered with finite volumes, having a grid point for the u-velocity in the middle of the west and east side and a grid point for the v-velocity in the middle of the north and south side of each volume. All other variables have their grid point in the centre of a volume. The equations are integrated over each volume, after which mass, momentum, T, k and ε fluxes are discretized with finite differences. We have discretized these convection terms with the hybrid scheme. This implies that the second-order accurate central scheme for the convection is locally replaced by the first-order accurate upwind scheme as soon as the grid size exceeds a critical value. In comparison with the use of the central scheme for all grid points, the hybrid scheme is more stable during the iteration process to solve the discretized system. We checked that continuation of the iteration process on the central scheme, after the solution for the hybrid scheme has been obtained, only leads to very small differences.

The appearance of boundary layers requires a non-equidistant grid that gives a strong grid refinement along the walls. The sides of the finite volumes are positioned according to

$$\frac{x_i}{H} = \tfrac{1}{2}\left(1 + \frac{\tanh\left[\alpha_1(i/i_{\max} - 1/2)\right]}{\tanh(\alpha_1/2)}\right), \qquad i = 0, 1, \ldots, i_{\max} \tag{3a}$$

$$\frac{y_j}{H} = \frac{j}{j_{\max}} - \frac{1}{2\pi}\sin\left(2\pi\frac{j}{j_{\max}}\right), \qquad j = 0, 1, \ldots, j_{\max} \tag{3b}$$

where α_1 is derived from the expression $\alpha_2 = \alpha_1/\sinh(\alpha_1)$, in which α_2 is chosen close to zero: the smaller α_2, the stronger the grid refinement along the vertical walls. The first inner grid point is approximately positioned at $x_1/H = \alpha_2/i_{max}$. In most calculations we took $\alpha_2 = 0.0015$.

The time dependence is treated implicitly; the spatial derivatives are evaluated at the new time level $n+1$, and the time derivatives are approximated with two time levels (B2 scheme)

$$\left(\frac{\partial\phi}{\partial t}\right)^{n+1} = \frac{\phi^{n+1}-\phi^n}{\Delta t} + O(\Delta t). \tag{4}$$

The discretized system at the new time level $n+1$ consists of non-linear, algebraic equations which are solved iteratively with a line Gauss–Seidel method. Alternating sweeps are made from the west to the east side and from the east to the west side of the computational domain. The updating of the iterative solution is such that only tridiagonal matrices have to be solved at a line. In each Gauss–Seidel sweep the variables u, v, T, k and ε are updated one after the other at a line. After each sweep the pressure is updated with a pressure-correction method. This method determines a pressure correction as long as the continuity equation in the finite volume is not satisfied: the pressure is increased/decreased as long as there is a net inflow/outflow of mass. The pressure correction is described by a Poisson equation

$$\frac{\partial^2 p'}{\partial x^2} + \frac{\partial^2 p'}{\partial y^2} = \frac{\rho}{\Delta t}\left(\frac{\partial u}{\partial x} + \frac{\partial v}{\partial y}\right). \tag{5}$$

This equation is solved with a direct solver. Discretization of equation (5) gives a symmetric band matrix for the Laplace operator, having fixed coefficients which only depend on the geometry. The LU decomposition of this matrix has to be determined only once and can be stored. The sweep process at the new time level is stopped when the pressure correction in each finite volume and the heat flux through the boundaries are below a certain criterion. Typically 5–10 sweeps at each time level are sufficient.

The calculation is started with a certain initial field at $t = 0$ and we integrate in time until a steady final solution is reached. The time evolution in the cavity is dominated by three time scales: $t_1 = H^2/\nu$, $t_2 = (H^2/\nu)Ra^{-1/4}$ and $t_3 = (H^2/\nu)Ra^{-1/2}$ (see ref. [15]). The conductive time scale t_1 determines the time to reach the steady state and t_3 determines the required time step; roughly $t_1/t_3 = Ra^{1/2}$ time steps are required to calculate the steady solution. For example the solution for Ra^{14} should require of the order of 10^7 time steps. This amount of time steps can considerably be reduced if we can get rid of the conductive time scale. This can be achieved by calculating an initial guess with the steady formulation. The unsteady terms are omitted and the transport variables are solved by the same Gauss–Seidel procedure as previously described. The equation for the pressure correction is obtained by using the SIMPLE method of Patankar and Spalding [16]. This equation is also solved iteratively with the Gauss–Seidel solver. Some underrelaxation is required to prevent divergence of the iteration process. After approximately 3000 Gauss–Seidel sweeps the speed of convergence has slowed down, and we switch over to the unsteady, more physical, formulation. The conductive time scale is already solved at the moment of switching and only the order of $t_2/t_3 = Ra^{1/4}$ time steps are required to reach the converged steady state. Indeed we find that for $Ra = 10^{14}$ roughly 4000 time steps are sufficient.

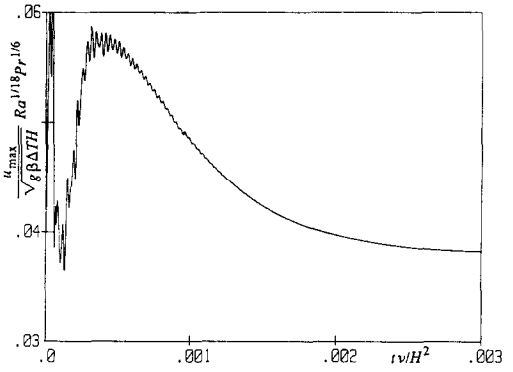

FIG. 2. Typical time evolution to the steady state (Chien model, air at $Ra = 10^{11}$).

As also found by Jones [17] and Thompson *et al.* [18], in the present calculations we revealed that the time scale t_3 (which is proportional to $H/\sqrt{(g\beta\Delta TH)}$, the Brunt–Väisälä time scale) determines the maximum time step that still gives a stable numerical time integration. In all cases we used $\Delta t\sqrt{(g\beta\Delta TH)}/H = 0.25$. A typical time evolution is shown in Fig. 2. In all calculations the damped oscillations are related to internal gravity waves in the core. For the turbulent solutions, almost irrespective of the Rayleigh number and Prandtl number, the frequency of the damped oscillations approximately is $fH/\sqrt{(g\beta\Delta TH)} = 0.087$. Ozoe *et al.* [8] have also calculated the turbulent flow in the same square cavity with the unsteady approach, using the k–ε model with wall functions. From their Fig. 13 we derive that the unsteady evolution shows oscillations with a frequency $fH/\sqrt{(g\beta\Delta TH)} = 0.083$ ($Ra = 6.3\times10^{10}$, $Pr = 6.7$; 24×60 grid, $\Delta t\sqrt{(g\beta\Delta TH)}/H \sim 1/12$). This value is close to our result. But in contrast with our results, the oscillations of Ozoe *et al.*, do not die out in the core for increasing time. We refined our time step up to $\Delta t\sqrt{(g\beta\Delta TH)}/H = 1/24$, and switched over to the central scheme, but still did not find their periodic behaviour for $t \to \infty$. In all cases the unsteadiness dies out and the turbulent solution reaches a steady final state. Both the use of a slightly different turbulence model or an insufficient numerical accuracy can account for the difference.

The use of low-Reynolds-number k–ε models requires a sufficient number of grid points in the inner

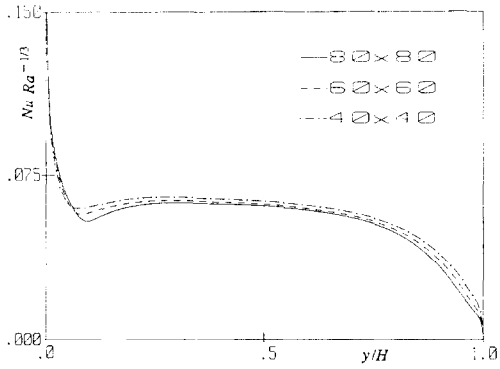

FIG. 3. Numerical accuracy of the wall-heat transfer (Chien model, air at $Ra = 10^{12}$).

part of the boundary layer. The different models lead to differences in the prediction of the wall-heat transfer of about 20%. Such differences can easily be lost if the number of grid points is too small and/or the grid points are not properly distributed. Figure 3 shows the wall-heat transfer for increasing grid refinement (40×40, 60×60, 80×80 grid). For example in the horizontal direction at half the cavity height, the 80×80 grid for air at $Ra = 10^{12}$ has about 30 grid points in each vertical boundary layer and about 20 grid points in the core. Within the vertical boundary layer 13 grid points are between the wall and the velocity maximum. For water at $Ra > 10^{13}$ refining the constant α_2 in equation (3a) from 0.0015 to 0.00015 increases the accuracy for a given number of grid points. All results which are presented in the sequel were obtained on the 80×80 grid. By repeating the calculations on the 60×60 grid, each result was checked to have only a small numerical error.

4. EXISTING EXPERIMENTAL AND NUMERICAL DATA

Accurate measurements for the turbulent natural-convection flow in the cavity are still difficult to obtain. For the comparison of the present numerical results with experiments, we have to rely on experiments performed in cavities with an aspect ratio (A = height/width) larger than 1. Cheesewright *et al.* [19] and Cheesewright and Ziai [20] obtained experimental data for air in the $A = 5$ cavity, MacGregor and Emery [21] measured a whole range of Prandtl numbers in large-aspect-ratio cavities (up to $A = 40$), Cowan *et al.* [22] measured the flow of water in large aspect-ratio cavities (up to $A = 60$) and Betts and Dafa'Alla [23] measured air in the $A = 30$ cavity.

At large Rayleigh numbers ($> 10^6$), boundary layers develop along the vertical sides. If for a certain large, but fixed, Rayleigh number the aspect ratio is increased, the rising boundary layer along the hot wall and the falling boundary layer along the cold wall will touch each other and the core region disappears. In the limit of $A \to \infty$ the flow becomes parallel (i.e. one-dimensional). Two-dimensional effects are restricted to a thin region close to the horizontal walls. The turbulence in this case reaches its maximum at the vertical centreline of the cavity. The flow in the large cavities as measured by MacGregor and Emery, Cowan *et al.* and Betts and Dafa'Alla are nearly parallel, giving an averaged wall-heat transfer

$$\overline{Nu} = c\, Ra^{1/3} \tag{6}$$

with the constant $c = 0.046$, 0.043 and 0.053, respectively. The Nusselt number (Nu) is the dimensionless heat transfer through the hot wall: $Nu = -H/\Delta T[\partial T/\partial x]_w$. The averaged Nusselt number according to equation (6) is independent of the aspect ratio. However, the boundary layers in the square cavity are not mixed up; the turbulence is concentrated in the boundary layers and is almost absent at the vertical centreline of the core. Therefore, the averaged wall-heat transfer in the square cavity might differ from equation (6). Cheesewright *et al.* [19] have measured velocity profiles for air as a function of height along both the hot and cold wall in an $A = 5$ cavity. In contrast with what follows under the Boussinesq assumption, the deviation from the centro-symmetric state in the experiments is relatively large. Cheesewright *et al.* contribute this deviation to heat losses through the horizontal walls, which were not perfectly adiabatic. Also three-dimensional effects might have influenced the experiment. The heat losses cause the horizontal boundary layer along the ceiling to become turbulent. The boundary layer along the floor is relaminarized, as in our calculations. The aspect ratio 5 is still small enough to have separated vertical boundary layers.

Comparison of different existing wall-heat transfer experiments for the vertical hot plate in an isothermal environment up to about $Ra = 10^{12}$ leads to (see ref. [4]) $Nu_y = 0.118 Ra_y^{1/3}$ (Nu and Ra are based on the coordinate y along the plate and on the temperature difference between the wall and the environment). Under the approximation that the core in the square cavity is also isothermal, this result can be rewritten as

$$\overline{Nu} = 0.047 Ra^{1/3}. \tag{7}$$

Here Nu and Ra are based on the cavity height H and twice the temperature difference between the hot wall and the isothermal core. But actually the core of the square cavity is stratified, which might give an averaged wall-heat transfer that differs from equation (7). For example, laminar calculations show that the stratification in the core leads to a 40% higher averaged wall-heat transfer for the cavity compared to the hot plate in an isothermal environment (see ref. [24]), $\overline{Nu} = 0.304 Ra^{1/4}$ and $0.218 Ra^{1/4}$ respectively for air. However, we will show that in the turbulent case the stratification in the core is more isothermal than in the laminar case. It is remarkable that the measured averaged wall-heat transfer for the plate (7) is close to the experimental relation for large-aspect-ratio cavi-

ties (6); equation (7) will be used for comparison with the numerical results in the square cavity.

Betts and Dafa'Alla calculated the cavity for an infinite aspect ratio, comparing different low-Reynolds-number k–ε models. In general, all these models predict a too high wall-heat transfer and a too low velocity maximum. In order to improve the performance of the Jones and Launder model, Ince and Launder [9] modified the E-term in the ε-equation with the Yap correction. This correction accounts for the large turbulent diffusion from the centreline of the tall cavity towards the wall. With the Yap correction, Ince and Launder calculated that $\overline{Nu} = 0.051 Ra^{1/3}$ for $A = \infty$. Further they used this modified model to calculate the cases with $A = 10$, 5 and 1. The Yap correction does not influence the results in the cases with $A = 5$ or 1, where the vertical boundary layers are not mixed up at the centreline. They fitted their numerical results for these finite aspect ratios to $\overline{Nu} = 0.047 Ra^{1/3}$. As shown in Fig. 4(a), their Rayleigh number in the case of the square cavity was too small to get a turbulent solution: their wall-heat transfer in this case is practically equal to our laminar result.

Markatos and Pericleous [7] and Ozoe *et al.* [8] calculated the turbulent flow in the square cavity, using the k–ε model with (logarithmic) wall functions. Ozoe *et al.* calculated the flow of water on a 24×60 grid. The distribution of grid points is such that only one grid point falls between the wall and the velocity maximum in the vertical boundary layer. Therefore, they do not claim that their results are grid independent. Their averaged wall-heat transfer at $Ra = 6.3 \times 10^{10}$ ($Pr = 6.7$) is indicated in Fig. 4(b). Markatos and Pericleous calculated air on a 60×120 grid. The distribution of grid points is such that 10–15 points fall in the vertical boundary layer, and care was taken that several of these points fall between the wall and the velocity maximum. They checked that grid refinement up to 100×160 points leads to small changes. Comparison of their wall-heat transfer results with the present results for the k–ε model with wall functions in Fig. 4(a) shows that our results are about 20% lower. Maybe this difference is a consequence of the slightly different formulation of the wall functions.

5. NUMERICAL RESULTS FOR AIR AND WATER

Laminar and turbulent solutions have been obtained for air ($Pr = 0.71$) up to $Ra = 10^{14}$ and for water ($Pr = 7.0$) up to $Ra = 10^{15}$. For the low-Reynolds-number models of Chien, and Jones and Launder, the solution in which k, ε and ν_t vanish everywhere satisfies equations (1) with its boundary conditions. This solution defines the laminar velocity and temperature field. As long as the Rayleigh number is below a certain critical value this laminar solution is steady and forms a unique solution of equations

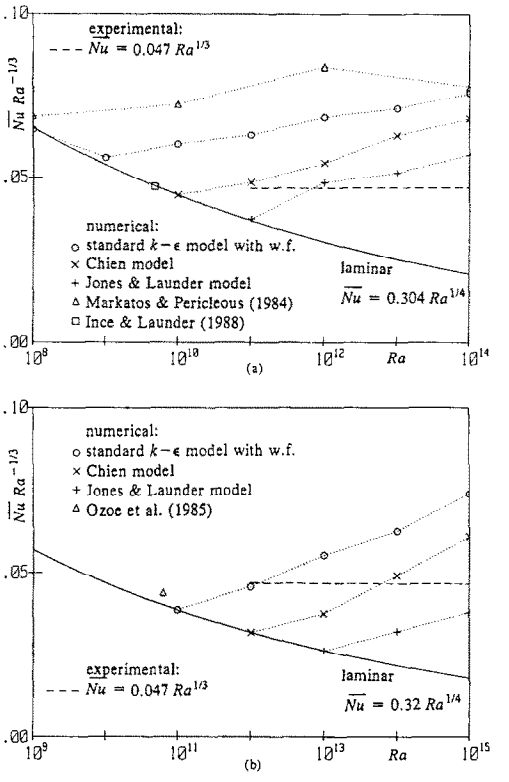

FIG. 4. Averaged wall-heat transfer: (a) air; (b) water.

(1). We switched off the turbulence model and calculated this laminar branch of solutions. For increasing Rayleigh number ($> 10^6$) the averaged wall-heat transfer for the laminar solution in Fig. 4 follows the asymptote $\overline{Nu} = 0.30 Ra^{1/4}$ for air and $\overline{Nu} = 0.32 Ra^{1/4}$ for water. If the turbulence model is included, the solution can leave the laminar branch for $Ra > Ra_{cr}$ and follows the turbulent branch: Ra_{cr} is a so-called bifurcation point of the equations. The averaged wall-heat transfer in Fig. 4 shows that Ra_{cr} depends on the turbulence model used. For air, the Chien model bifurcates at $Ra_{cr} \sim 10^{10}$ and the Jones and Launder model at $Ra_{cr} \sim 10^{11}$. Increasing the Prandtl number delays the bifurcation: for water, the Chien model bifurcates at $Ra_{cr} \sim 10^{12}$ and the Jones and Launder model at $Ra_{cr} \sim 10^{13}$. The standard k–ε model with wall functions shows the earliest transition to turbulence, namely at $Ra_{cr} \sim 10^9$ for air and at $Ra_{cr} \sim 10^{11}$ for water.

When the standard k–ε model is used, the laminar solution (with zero turbulent viscosity) is not a solution of equations (1), because it does not satisfy the boundary condition (wall function) for the kinetic energy at the first inner grid point. We calculate that below a critical Rayleigh number the standard k–ε model gives a turbulent viscosity which is close to zero everywhere. This solution can be interpreted as an approximation of the laminar flow. Above the critical value the turbulent viscosity suddenly increases and a turbulent solution is found. This sudden increase is also seen in the wall-heat transfer for the standard k–

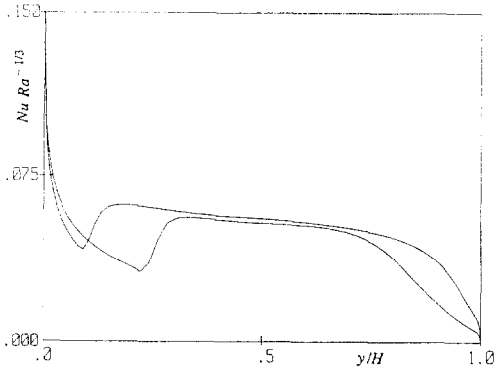

FIG. 5. Non-uniqueness of the turbulent solution (Jones and Launder model, air at $Ra = 10^{13}$, 80×80 grid).

ε model in Fig. 4. Because we cannot prove that the (nearly) laminar branch in the standard k–ε model still exists for $Ra > Ra_{cr}$, as is trivial for the low-Reynolds-number models, it is not certain that the standard k–ε model contains a bifurcation point.

Examining the development of the wall-heat transfer along the hot vertical side of the cavity in Fig. 5 shows a sudden increase beyond a critical height (y_{tr}). This increase represents the laminar–turbulent transition. Some of our calculations show that the position of the turbulent transition is not uniquely given as a function of Pr and Ra. The position depends on the initial solution at $t = 0$ with which the evolution to the steady state is started. For example at the same 80×80 grid we calculate two different solutions for air at $Ra = 10^{13}$ with the Jones and Launder model (see Fig. 5): the one with an early and the other with a late transition. We have carefully checked the convergence to the steady state for both solutions. The difference between the laminar part of both solutions is related to a difference in the core stratification. The non-uniqueness of the transition region is also found in the experiments of Jaluria and Gebhart [25] (and private communication with Gebhart) for the hot vertical plate in an isothermal environment. We expect that for a fixed Rayleigh number even more than the two partly turbulent solutions we found can exist: probably y_{tr} can be anywhere between a minimum distance (below which the solution is always laminar) and a maximum distance (beyond which the solution is always turbulent). The minimum distance equals H if the Rayleigh number is below Ra_{cr} and the maximum distance reaches zero if the Rayleigh number is sufficiently far beyond Ra_{cr}. Hence, for very large Rayleigh numbers the boundary layer is fully turbulent. A late transition decreases the averaged wall-heat transfer; for each Rayleigh number in Fig. 4 we have selected the averaged wall-heat transfer of the solution with the lowest position of transition, in cases where multiple solutions were calculated. It is interesting to note that also for the standard k–ε model non-uniqueness was found: for example two solutions were calculated for air at $Ra = 10^{9.75}$ using the 60×60 grid. The non-uniqueness of the turbulent solution in the transition regime for the standard k–ε model supports the suggestion that also this model, like the low-Reynolds-number models, has a bifurcation point at Ra_{cr}.

The gradient of the vertical temperature profile in the centre of the cavity ($S = H/\Delta T[\partial T/\partial y]$) is shown in Fig. 6 as a function of the Rayleigh number. The laminar branch is calculated by switching off the turbulence model. For completeness we have also calculated the solution for small Rayleigh numbers. When the Rayleigh number is close to zero there is only conduction, giving a zero vertical temperature gradient. Beyond $Ra = 10^6$ the temperature in the core becomes stratified, and the gradient in the centre follows the asymptote $S = 1.0$ (for air). If the standard k–ε model is used, the stratification leaves the laminar branch at about $Ra = 10^9$. In the transition region the stratification increases sharply, after which it falls back to values below the laminar solution. For increasing Rayleigh number the stratification for the turbulent solution is broken up. Extrapolation suggests that it totally vanishes for infinitely large Rayleigh numbers, according to the asymptote (for air)

$$\lim_{Ra\to\infty} \frac{H}{\Delta T}\frac{\partial T}{\partial y}\bigg|_{\text{centre}} = 2.266\, Ra^{-1/16} \tag{8a}$$

or

$$\lim_{Ra\to\infty} \frac{T - T_h}{\Delta T}\bigg|_{\text{core}} = \tfrac{1}{2} + 2.266\left(\frac{y}{H} - \tfrac{1}{2}\right) Ra^{-1/16}. \tag{8b}$$

Figure 6 also gives an experimental value of the stratification as found by Cheesewright *et al.* [19] for air in the $A = 5$ cavity. This value is close to that of the calculation. The stratification for water is roughly a factor 2 smaller than for air. Deviations in the stratification between the different turbulence models are small.

The small stratification in the turbulent case motivates a comparison with the hot vertical plate in an isothermal environment. As already mentioned in the previous paragraph, $\overline{Nu} = 0.047 Ra^{1/3}$ fits both the experiment for the hot vertical plate and for the tall vertical cavity. For air (see Fig. 4(a)) the Jones and

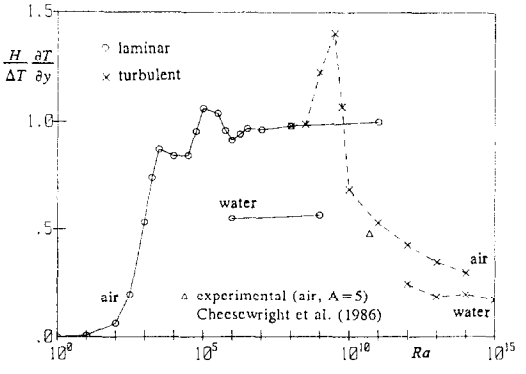

FIG. 6. Thermal stratification in the centre of the core (standard k–ε model with wall functions is used in the turbulent case).

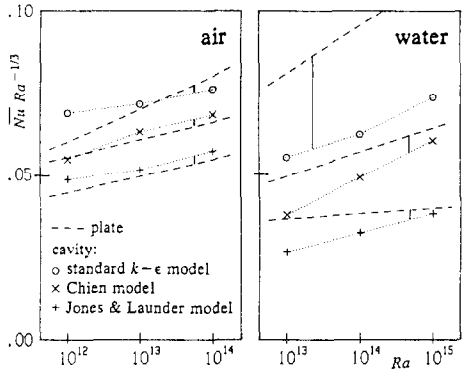

FIG. 7. Comparison of the averaged wall-heat transfer between the cavity and the plate.

Launder model is closest to this experiment, the Chien model is a bit too high and the standard k–ε model is much too high. Also for water (see Fig. 4(b)) the standard k–ε model gives a too high wall-heat transfer, whereas the Chien model and the Jones and Launder model are reasonably close to the experiment. Indeed, the agreement for none of the models is extremely well. However, there is both an error in the experiment itself as an error due to the comparison with experiments in related configurations instead of the square cavity itself. It is clear that there is a strong need for accurate measurements in the square cavity for the high-Rayleigh-number fully turbulent regime. In Fig. 7 we have compared the calculated averaged wall-heat

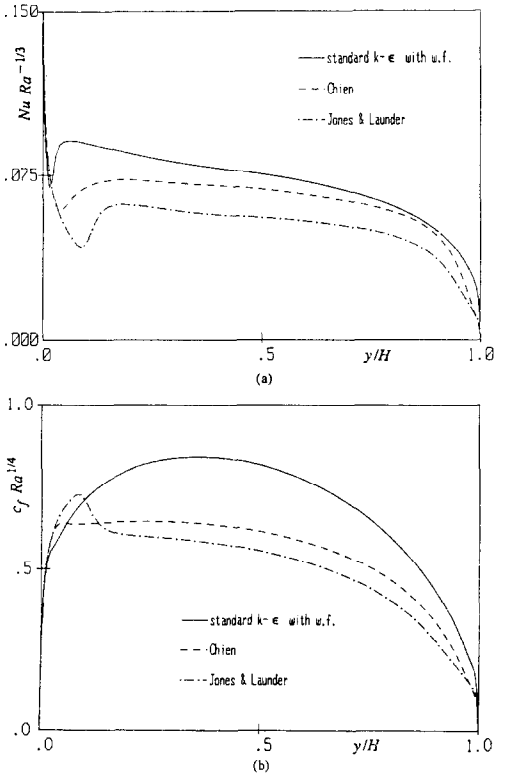

FIGS. 8(a) and (b).

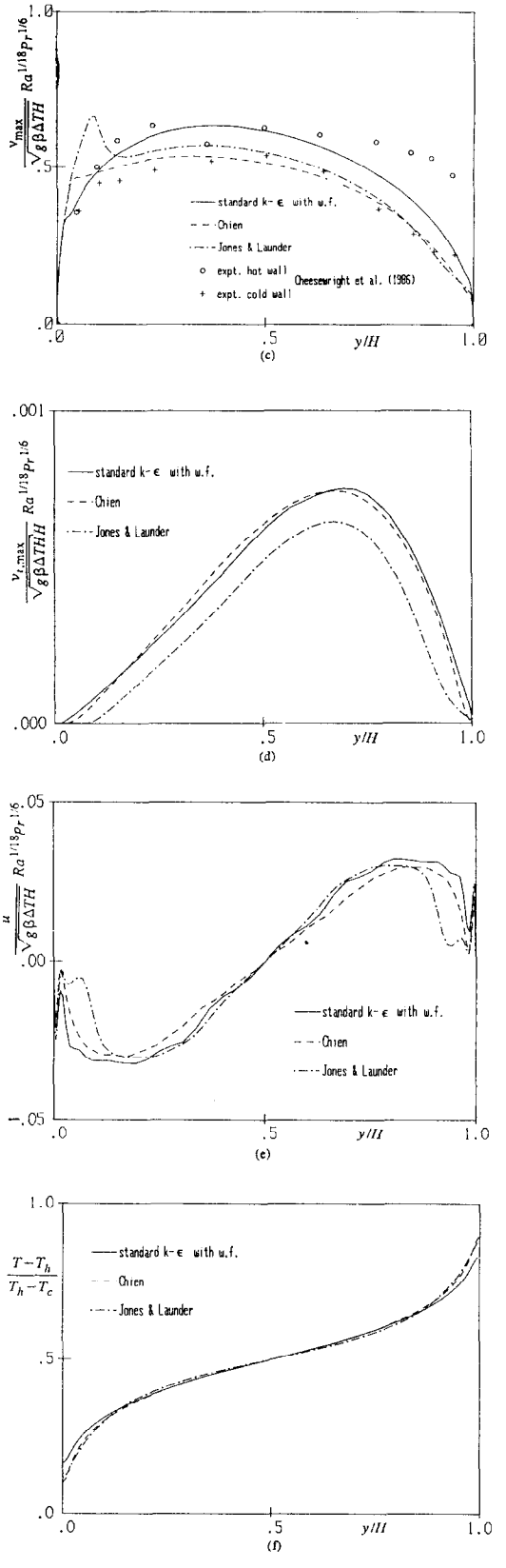

FIG. 8. Comparison of different turbulence models for air at $Ra = 10^{13}$: (a) wall-heat transfer; (b) wall-shear stress; (c) vertical velocity maximum; (d) turbulent viscosity maximum; (e) horizontal velocity at $x = H/2$; (f) thermal stratification at $x = H/2$.

transfer for each model in the cavity with the result for the same model at the hot vertical plate [4]. The characteristic temperature for the plate is taken as $2(T_h - T_c)$, in which T_c is the environment temperature. For air the agreement between the cavity and plate result for each model is close, but for water the deviation is larger, in particular for the standard k–ε model. One should expect the opposite, because for a given Rayleigh number the stratification for water is closer near the isothermal state than for air. However, a nearly isothermal core does not guarantee that the wall-heat transfer for the cavity is the same as for the plate: also the horizontal walls influence the development of the vertical boundary layer.

In Fig. 8 we have compared several quantities, as calculated by the different turbulence models, as a function of height for air at $Ra = 10^{13}$: wall-heat transfer, wall-shear stress, maximum of the vertical velocity, maximum of the turbulent viscosity, horizontal velocity at half the cavity width and the thermal stratification at half the cavity width. In this figure the dimensionless wall-shear stress is defined as

$$c_f = \frac{2\nu}{g\beta\Delta TH}\left(\frac{\partial v}{\partial x}\right)_w. \tag{9}$$

All the quantities are scaled such that the turbulent solution is almost independent of the Rayleigh number. These scalings are consistent with those we formulated in ref. [3] for the hot vertical plate. Figure 8 shows that the differences between the turbulence models are largest for the wall-heat transfer and the wall-shear stress. These quantities belong to the inner layer of the vertical boundary layer, i.e. the layer from the wall up to the velocity maximum. Differences for the vertical velocity maximum are small. The calculated velocity maximum is reasonably close to the experiment of Cheesewright *et al.* [19] for air at $Ra = 5 \times 10^{10}$ in the $A = 5$ cavity. Differences between the models for quantities in the outer layer of the vertical boundary layer are small. For example the small difference in the maximum of the turbulent viscosity as calculated by the Jones and Launder model is due to the slightly later transition of this model. The later transition of the Jones and Launder model is also recognizable in the horizontal velocity at half the cavity width as shown in Fig. 8(e). For increasing height in this figure we find (modulus value of the horizontal velocity is considered): (i) a thin high-speed horizontal boundary layer close to the floor, (ii) the velocity falls back to an almost zero value directly outside the horizontal boundary layer, and (iii) at the height of the transition the horizontal velocity suddenly increases, reaches a maximum and becomes zero in the centre. The increase of the horizontal velocity is related to the sudden thickening of the boundary layer at the laminar–turbulent transition position demanding a larger inflow of fluid from the environment. The thermal stratification in the core (Fig. 8(f)) is linear, except close to the horizontal walls. Figure 9 compares the wall-heat transfer and velocity maximum for water. Differences between the wall-heat transfer are largest.

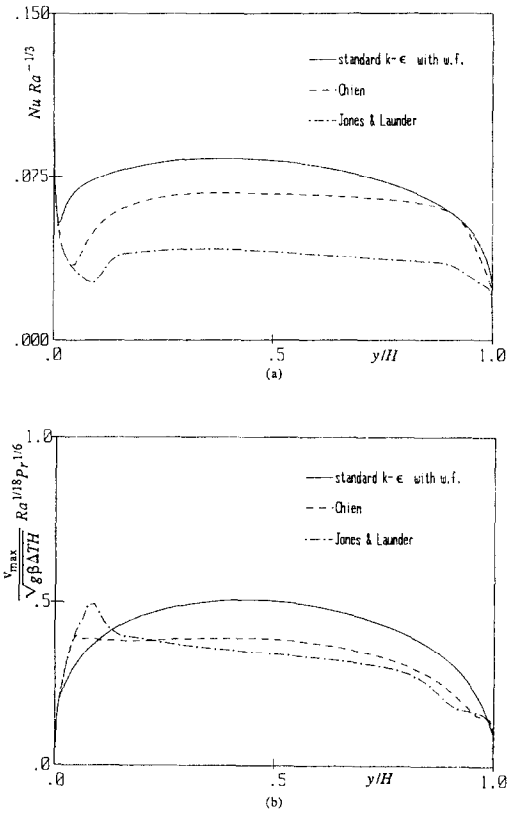

FIG. 9. Comparison of different turbulence models for water at $Ra = 10^{15}$; (a) wall-heat transfer; (b) vertical velocity maximum.

6. CONCLUSION

Fine grids (up to 80×80 points) and a proper distribution of the grid points (with a strong concentration in the vertical boundary layers) are required to get an accurate numerical solution for the high-Rayleigh-number laminar and turbulent natural-convection flow in the square cavity heated from the vertical side.

Below a critical Rayleigh number (Ra_{cr}) the solution is laminar everywhere. Increasing the Prandtl number increases Ra_{cr}: the standard k–ε model finds $Ra_{cr} \sim 10^9$ for air and $Ra_{cr} \sim 10^{11}$ for water. The low-Reynolds-number k–ε models find higher values. The Jones and Launder model remains laminar even to $Ra_{cr} \sim 10^{11}$ for air and to $Ra_{cr} \sim 10^{13}$ for water. Ra_{cr} is a bifurcation point of the flow equations using a low-Reynolds-number k–ε model. For all turbulence models used (standard k–ε model, Chien model and Jones and Launder model) multiple (partly) turbulent solutions were calculated on the same grid and at a fixed Rayleigh number above Ra_{cr}. This refers to the non-uniqueness of the position of the laminar–

turbulent transition in the vertical boundary layer. All the models uniquely determine the fully turbulent solution at the highest Rayleigh numbers we considered.

The laminar solution at high Rayleigh numbers ($>10^6$) shows a thermal stratification in the core which is almost independent of the Rayleigh number. When the flow becomes turbulent, the stratification decreases with increasing Rayleigh number and seems to vanish totally for infinitely large Rayleigh numbers. The nearly isothermal core suggests a comparison of the averaged wall-heat transfer for the turbulent flow in the cavity with the wall-heat transfer for the hot vertical plate in an isothermal environment. Indeed deviations are small for air, but they are larger for water. Comparison with both the experiment for the plate and for tall vertical cavities shows that the prediction for the averaged wall-heat transfer by the standard k–ε model is too high, whereas the low-Reynolds number models of Chien, and Jones and Launder are reasonably close to the experiment. A more definitive conclusion about the accuracy of the different models requires the availability of accurate measurements in the square cavity at $Ra > 10^{12}$.

Differences between the turbulence models are largest for quantities that are determined in the inner layer of the vertical boundary layer, for example the wall-heat transfer and the wall-shear stress. Differences for the vertical velocity maximum, the turbulent viscosity maximum, the horizontal velocity at half the cavity width and the thermal stratification in the core are small. Differences between the models are larger for water than for air.

REFERENCES

1. W. K. George and S. P. Capp, A theory for natural convection turbulent boundary layers next to heated vertical surfaces, *Int. J. Heat Mass Transfer* **22,** 813–826 (1979).
2. R. Cheesewright, The scaling of turbulent natural convection boundary layers in the asymptotic limit of infinite Grashof number. Paper presented at the Euromech Colloquium 207, 7–9 April, Delft, The Netherlands (1986).
3. R. A. W. M. Henkes and C. J. Hoogendoorn, Numerical determination of wall functions for the turbulent natural convection boundary layer, *Int. J. Heat Mass Transfer* **33,** 1087–1097 (1990).
4. R. A. W. M. Henkes and C. J. Hoogendoorn, Comparison of turbulence models for the natural convection boundary layer along a heated vertical plate, *Int. J. Heat Mass Transfer* **32,** 157–169 (1989).
5. K.-Y. Chien, Predictions of channel and boundary layer flows with a low-Reynolds-number two-equation model of turbulence, AIAA-80-0134 (1980).
6. W. P. Jones and B. E. Launder, The prediction of laminarization with a two-equation model of turbulence, *Int. J. Heat Mass Transfer* **15,** 301–314 (1972).
7. N. C. Markatos and K. A. Pericleous, Laminar and turbulent natural convection in an enclosed cavity, *Int. J. Heat Mass Transfer* **27,** 755–772 (1984).
8. H. Ozoe, A. Mouri, M. Ohmuro, S. W. Churchill and N. Lior, Numerical calculations of laminar and turbulent natural convection in water in rectangular channels heated and cooled isothermally on the opposing vertical walls, *Int. J. Heat Mass Transfer* **28,** 125–138 (1985).
9. N. Z. Ince and B. E. Launder, Computation of turbulent natural convection in closed rectangular cavities, 2nd U.K. Natn. Conf. on Heat Transfer, Glasgow, pp. 1389–1400 (1988).
10. W. Rodi, Turbulence models and their application in hydraulics, a state of the art review, Int. Ass. for Hydraulic Research, Delft, The Netherlands (1980).
11. M. P. Fraikin, J. J. Portier and C. J. Fraikin, Application of a k–ε turbulence model to an enclosed buoyancy driven recirculating flow, *Chem. Engng Commun.* **13,** 289–314 (1982).
12. P. R. Nachtsheim, Stability of free-convection boundary-layer flows, NASA TN D-2089 (1963).
13. P. G. Drazin and H. W. Reid, *Hydrodynamic Stability.* Cambridge University Press, London (1981).
14. T. W. J. Peeters and R. A. W. M. Henkes, The Reynolds-stress model of turbulence applied to the natural-convection boundary layer along a heated vertical plate, *Int. J. Heat Mass Transfer* (1991), in press.
15. R. A. W. M. Henkes and C. J. Hoogendoorn, On the stability of the natural convection flow in a square cavity heated from the side, *Appl. Scient. Res.* **47,** 195–220 (1990).
16. S. V. Patankar and D. B. Spalding, A calculation procedure for heat, mass and momentum transfer in three dimensional parabolic flows, *Int. J. Heat Mass Transfer* **15,** 1787–1806 (1972).
17. I. P. Jones, The convergence of a simple iterative strategy for strongly stratified flows. In *Numerical Methods on Laminar and Turbulent Flow* (Edited by C. Taylor), pp. 733–740. Pineridge Press, Swansea (1985).
18. C. P. Thompson, N. S. Wilkes and I. P. Jones, Numerical studies of buoyancy-driven turbulent flow in a rectangular cavity, *Int. J. Numer. Meth. Engng* **24,** 89–99 (1987).
19. R. Cheesewright, K. J. King and S. Ziai, Experimental data for the validation of computer codes for the prediction of two-dimensional buoyant cavity flows, *HTD* **60,** 75–81 (1986).
20. R. Cheesewright and S. Ziai, Distributions of temperature and local heat-transfer rate in turbulent natural convection in a large rectangular cavity, *Proc. 8th Int. Heat Transfer Conf.*, San Francisco, pp. 1465–1470 (1986).
21. R. K. MacGregor and A. F. Emery, Free convection through vertical plane layers—moderate and high Prandtl number fluids, *J. Heat Transfer* **91,** 391–403 (1969).
22. G. H. Cowan, P. C. Lovegrove and G. L. Quarini, Turbulent natural convection heat transfer in vertical single water-filled cavities, *Proc. 7th Int. Heat Transfer Conf.*, München, Vol. 2, pp. 195–204 (1982).
23. P. L. Betts and A. A. Dafa'Alla, Turbulent buoyant air flow in a tall rectangular cavity, *HTD* **60,** 83–91 (1986).
24. R. A. W. M. Henkes, A. M. Lankhorst and C. J. Hoogendoorn, Structure of the laminar natural convection flow in a square cavity heated from the side for infinitely large Rayleigh number, *Proc. ASME Winter Annual Meeting, Natural Convection in Enclosures*, HTD-99, pp. 9–16 (1988).
25. Y. Jaluria and B. Gebhart, On transition mechanisms in vertical natural convection flow, *J. Fluid Mech.* **66,** 309–337 (1974).

CONVECTION NATURELLE DANS UNE CAVITE CARREE, CALCULEE AVEC DES MODELES DE TURBULENCE A FAIBLE NOMBRE DE REYNOLDS

Résumé—La convection naturelle laminaire et turbulente dans une cavité bidimensionnelle carrée chauffée sur un coté vertical est calculée numériquement jusqu'à 10^{14} pour le nombre de Rayleigh sur l'air et 10^{15} sur l'eau. Trois différents modèles de turbulence sont comparés: le modèle classique k–ε avec fonction de paroi logarithmique et les modèles à faible nombre de Reynolds de Chien et Jones et de Launder. La position de la transition laminaire–turbulent dans la couche limite verticale dépend fortement du modèle de turbulence utilisé. Les solutions multiples pour la position de transition peuvent apparaître pour un nombre de Rayleigh donné, avec la même grille numérique. La stratification thermique dans le coeur de la cavité se rompt quand l'écoulement devient turbulent. Une comparaison, avec l'épaisseur, du transfert moyen sur la paroi chaude pour des cavités verticales hautes montre que le modèle standard k–ε donne une prédiction trop forte, tandis que les modèles à faible nombre de Reynolds sont raisonnablement proches de l'expérience.

BERECHNUNG DER NATÜRLICHEN KONVEKTION IN EINEM QUADRATISCHEN HOHLRAUM MIT HILFE VON TURBULENZMODELLEN FÜR KLEINE REYNOLDS-ZAHLEN

Zusammenfassung—Die laminare und turbulente natürliche Konvektionsströmung in einem zweidimensionalen quadratischen, seitlich beheizten Hohlraum wird numerisch für Rayleigh-Zahlen bis zu 10^{14} (für Luft) bzw. 10^{15} (für Wasser) berechnet. Es werden drei unterschiedliche Turbulenzmodelle verglichen: das Standard k–ε-Modell mit logarithmischen Wandfunktionen sowie die Modelle für kleine Reynolds-Zahlen von Chien und Jones/Launder. Die Stelle des Übergangs zwischen laminarer und turbulenter Strömung der senkrechten Grenzschicht hängt stark von dem verwendeten Turbulenzmodell ab. Außerdem können bei der Berechnung der Stelle des Übergangs für eine bestimmte Rayleigh-Zahl in ein und demselben numerischen Gitter Mehrfachlösungen auftreten. Die thermische Schichtung im Kern des Hohlraums wird zerstört, sobald die Strömung turbulent wird. Ein Vergleich des mittleren Wärmeübergangs an der Wand mit Versuchsergebnissen für eine heiße senkrechte Platte und für schlanke senkrechte Hohlräume zeigt, daß das Standard k–ε-Modell zu große Werte liefert, während die Modelle für kleine Reynolds-Zahlen die Versuchsergebnisse recht gut wiedergeben.

РАСЧЕТ ЕСТЕСТВЕННОКОНВЕКТИВНОГО ТЕЧЕНИЯ В КВАДРАТНОЙ ПОЛОСТИ С ИСПОЛЬЗОВАНИЕМ МОДЕЛЕЙ ТУРБУЛЕНТНОСТИ С НИЗКИМ ЧИСЛОМ РЕЙНОЛЬДСА

Аннотация—Ламинарное и турбулентное естественноконвективное течение в двумерной квадратной полости, нагреваемой со стороны вертикальной стенки, рассчитывается численно для значений чисел Рэлея вплоть до 10^{14} для воздуха и 10^{15}—для воды. Сравниваются три различные модели турбулентности: стандартная k–ε модель с логарифмическими функциями стенки, модели Чина, а также Джонса и Лондера с низким числом Рейнольдса. Расположение перехода от ламинарного течения к турбулентному в вертикальном пограничном слое в большой степени зависит от используемой модели турбулентности. Кроме того, для фиксированного числа Рэлея при одинаковой численной сетке могут существовать множественные решения расположения перехода. При турбулизации течения тепловая стратификация в ядре полости нарушается. Сопоставление усредненного теплопереноса от стенки с экспериментальными данными показывает, что стандартная k–ε модель дает весьма завышенные значения, в то время как модели с низким числом Рейнольдса позволяют получить результаты, близкие к экспериментальным данным.